

Using deep Residual Network to search for galaxy- $\text{Ly}\alpha$ emitter lens candidates based on spectroscopic-selection

Rui Li^{1,2,4*}, Yiping Shu^{5,6†}, Jianlin Su⁷, Haicheng Feng^{1,2,3,4}, Jiancheng Wang^{1,2,3,4‡}

¹ Yunnan Observatories, Chinese Academy of Sciences, 396 Yangfangwang, Guandu District, Kunming, 650216, P. R. China

² University of Chinese Academy of Sciences, Beijing, 100049, P. R. China

³ Center for Astronomical Mega-Science, Chinese Academy of Sciences, 20A Datun Road, Chaoyang District, Beijing, 100012, P. R. China

⁴ Key Laboratory for the Structure and Evolution of Celestial Objects, Chinese Academy of Sciences, 396 Yangfangwang, Guandu District, Kunming, 650216, P. R. China

⁵ Purple Mountain Observatory, Chinese Academy of Sciences, 2 West Beijing Road, Nanjing, Jiangsu, 210008, China

⁶ Institute of Astronomy, University of Cambridge, Madingley Road, Cambridge CB3 0HA, UK

⁷ School of Mathematics, Sun Yat-sen University, Guangzhou, China

Accepted XXX. Received YYY; in original form ZZZ

ABSTRACT

More than one hundred galaxy-scale strong gravitational lens systems have been found by searching the emission lines coming from galaxies with higher redshift than the foreground galaxies. Based on this spectroscopic-selection method, we introduce the Deep Residual Network (Resnet, one kind of deep Convolutional Neural Networks) to search the galaxy- $\text{Ly}\alpha$ emitter (LAEs) lens candidates by recognizing the $\text{Ly}\alpha$ emissions from the redshift of $2 < z < 3$ in the Data Release 12 (DR12) of the Baryon Oscillation Spectroscopic Survey (BOSS) of the Sloan Digital Sky Survey III (SDSS-III). In our study, we first build a 28 layers Resnet model and then artificially synthesize 150,000 spectra, including 140,000 spectra without $\text{Ly}\alpha$ emissions and 10,000 with $\text{Ly}\alpha$ emissions, to train it. After 25 epochs training, We obtain a near-perfect test accuracy of 0.9954 for our model, and the corresponding loss is 0.0028. We then apply our Resnet model to our predictive data contained with 174 known lens candidates. Finally we obtain 1232 hits including 161 (92.5%) of the 174 known candidates. Apart from the hits found in other works, our Resnet model also find 536 new hits. We then perform several subsequent selections to these 536 hits and present 6 most believable lens candidates in this paper.

Key words: gravitational lensing; strong - galaxies: elliptical - galaxies:structure

1 INTRODUCTION

Galaxy-scale strong gravitational lenses, which could provide very tight constraints on the projected mass of the lens galaxies, are not only available probes to research the structures, the formation and evolution of galaxies (e.g., Koopmans et al. (2006); Auger et al. (2010); Sonnenfeld et al. (2013), Bolton et al. (2012)), but also a crucial technique to studying the cosmology, for example, Suyu et al. (2013) made an blind analysis to the time-delay lens system RX J1131-1231 and successfully quantified the Hubble ctry toonstant H_0 with lower uncertainty ($H_0 = 78.7^{+4.3}_{-4.5}$). Additionally, gravitational lenses could act

as natural telescopes and give us magnified views of the background objects, which could help us to study the celestial body in the distant universe(e.g., Impellizzeri et al. (2008); Swinbank et al. (2009); Treu et al. (2015).

People have putted forward several techniques to search for the galaxy-scale strong gravitational lenses. One of the techniques is based on the arc-like shapes of the lens systems and many algorithm have been developed to find this arc-like morphological feature (Lenzen et al. 2004; Horesh et al. 2005; Seidel & Bartelmann 2007; Kubo & Dell’Antonio 2008; More et al. 2012). Another similar, but modified method comes from Gavazzi et al. (2014). They first subtracted the light of the central galaxies using multi-band images and then found the arc-like shapes in the residual images to confirm whether the targets are lens systems. On the basis of this work, Joseph et al. (2014) presented an PCA (Principal Component Analysis) algorithm to sub-

* E-mail: lirui@ynao.ac.cn

† E-mail: yiping.shu@pmo.ac.cn

‡ E-mail: jcwang@ynao.ac.cn

tract galaxies from imaging data and then found gravitational lenses in the resulting residual images. They pointed out that the PCA-based galaxy subtraction algorithm performs better than traditional galaxy subtraction based on model fitting.

Besides the method based on morphological classification, [Warren et al. \(1996\)](#) for the first time proposed a spectroscopic-selection technique. This technique identifies the lens candidates by looking for compound spectra. As shown in Figure 2, the left spectrum is a compound spectrum of an identified lensing system, SDSSJ 1110+2808. The foreground galaxy of this lens system is an early-type galaxy (ETG) and its spectrum has no emissions in the band of $< \lambda < 5000\text{\AA}$. However, near the wavelength of 4150\AA we can find an emission line which in fact is a Ly α emission coming from a Ly α emitter. The Ly α emitter lies close to the line of sight of the ETG and with a redshift of $z = 2.3999$, which indicates that the light from the Ly α emitter is likely to be deflected by the gravitation of the foreground galaxy and thus form several images around the foreground galaxy. Simply speaking, the spectroscopic-selection technique searches the spectrum of a targeted galaxy showing evidences of emissions from a background source and then follow-up high-resolution image observations to confirm the lens nature. Further detail description of this technique could be found in ([Bolton et al. 2004](#)). Using this technique, researches have conducted several galaxy-scale strong lens surveys, such as the Sloan Lens ACS (SLACS; [Bolton et al. \(2006, 2008\)](#)) survey, the Sloan WFC Edge-on Late-type Lens Survey (SWELLS; [Treu et al. \(2011\)](#)), the Baryon Oscillation Spectroscopic Survey (BOSS) Emission-Line Lens Survey (BELLS; [Bolton et al. \(2012\)](#)), the SLACS for the Masses (S4TM; [Shu et al. \(2015\)](#)) and the BELLS for the GALaxy-Ly α Emitter sYstems (BELLS GALLERY, [Shu et al. \(2016b\)](#)) survey. These surveys have totally found several hundreds galaxy-galaxy strong gravitational lenses and have generated numerous substantial studies about the structures, the formation and evolution of the early-type galaxies (ETGs) ([Koopmans et al. \(2006\)](#); [Auger et al. \(2009\)](#); [Bolton et al. \(2012\)](#); [Shu et al. \(2015\)](#)). Recently, using a similar spectroscopic-selection technique, [Meyer et al. \(2017\)](#) have found a sample of 9 secure QSO-Galaxy lens candidates, which demonstrates the potential application of the spectroscopic-selection technique in finding QSOs Lens. This spectroscopic-selection technique is the most efficient method so far. However, the speed of the codes is not fast enough, especially in the coming age of the big data of astronomy.

Several years ago, the Convolutional Neural Networks (CNNs) which is a kind of machine learning algorithm particularly suitable for image recognition tasks, have been applied in astronomy. The first application of CNNs is the spectral classification of the tenth data release (DR10) of the Sloan Digital Sky Survey (SDSS). [Hála \(2014\)](#) applied his CNNs model on more than 60000 spectra of SDSS and yielded success rate of nearly 95%. His work conclusively proved great potential of CNNs and deep learning methods in astrophysics. Later, the CNNs have been applied to many other works, such as the morphological classification of SDSS galaxies ([Dieleman et al. 2015](#)), the photometric redshifts estimation of SDSS galaxies ([Hoyle 2016](#)) and the star/galaxy classification ([Kim & Brunner 2017](#)). As for the

field of gravitational lenses, [Petrillo et al. \(2017\)](#) for the first time use the CNNs to recognize galaxy-scale strong gravitational lenses based on morphological classification. They successfully find 761 strong-lens candidates in the Kilo Degree Survey (KiDS) and after manual selection they presented 56 most reliable candidates in their paper.

However, the CNNs has not been applied for the searching of gravitational candidates based on the spectroscopic-selection technique. In this paper, we will use the Deep Residual Network (Resnet, one popular model of CNNs) to find the galaxy-Ly α emitter (LAEs) lens candidates by recognizing the Ly α emissions from the redshift of $2 < z < 3$ in the DR12 of SDSS. LAEs is a kind of young, low-mass galaxies with extremely star-formation. they are an important component of the early universe, and are critical for studying the formation and evolution of galaxies at that time. On the one hand, benefited from the magnifying effect of the gravitational lenses, LAEs lens can provide us good opportunities to study the LAEs themselves. On the other hand, LAEs lens can help us to exploit the small-scale dark substructure in the location of the lensed LAEs images and to constrain the slope and normalization of the substructure-mass function. As for why the galaxy-LAEs lens are suitable for constraining the substructure-mass function, [Shu et al. \(2016a\)](#) have discussed it carefully.

The paper is organized as follows. In Section 2, we will provide a brief description of CNNs and Resnet. In Section 3, we will talk about how to use Resnet to recognize emissions that are not coming from the foreground galaxies themselves. In this section, we also apply our algorithm to the DR12 of SDSS and compare our results with previous work of [Shu et al. \(2016a\)](#). In Section 4, we will present another 17 gravitational lens candidates found by our algorithm. In Section 5, we will discuss the advantages and the possible improvement of our strategy.

2 WHAT ARE CNNs AND RESNET

Recent years, CNNs have gained a lot of attentions in image recognition, speech recognition, motion analysis, nature language processing and many other researching fields. CNNs are a kind of deep feedforward neural networks with multiple different layers. The layers mainly contain the convolutional layers, the pooling layers and the fully-Connected layers. The convolutional layers contain lots of filters and aim to extract different feature of the input; The Pooling layers can compress the feature maps and simplify the calculations; The fully-Connected layers turn all the local feature maps into a global feature map. There are a lot of feature maps in each layers and each feature map can extract one feature by the convolution neurons. Usually, a feature map has several convolution neurons and the convolution neurons are composed of weights and bias which could be trained using the train data. During the training process, every convolution neuron can accept some inputs and do some convolution calculation.

A deep CNNs model could be designed as a classifier or be used to achieve a recognition tasks. Many evidences shows that the network depth is very important for the results of the classification and the recognition tasks. Theoretically, the train result should be better with the lay-

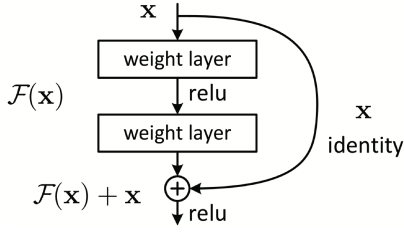


Figure 1. Residual learning: a building block with a shortcut connection

ers becoming deeper. However, for deeper networks, when they start converging, a “degradation” problem would occur: with the networks becoming deeper, accuracy gets saturated and then degrades rapidly (He et al. 2015), which is not caused by over fitting. That’s why many popular CNNs models have only a few layers (e.g., LeNet has 5 layers, Lecun et al. (1998); AlexNet has 7 layers, AlexNet, Krizhevsky et al. (2012)). In order to overcome the degradation of the accuracy with depth increasing, He et al. (2015) proposed a new CNNs model: the Deep Residual Network (Resnet).

ResNet assumes that it is easier to optimize the residual mapping than to optimize the origin, unreferenced mapping. Denoting the desired underlying mapping as $H(x)$ which would be fit by a few stacked layers, and x is the inputs of the first of these layers. They let the stacked layers fit the residual mapping of $F(x) := H(x) - x$. Then the original mapping $H(x)$ becomes $F(x) + x$, and it could be realized by feedforward neural networks with “shortcut connections” (see Figure 1) which simply perform the identity mapping then skip one or more layers and add their outputs to the outputs of the stacked layers. In He et al. (2015), the authors explained that “With the residual learning reformulation, if identity mappings are optimal, the solvers may simply drive the weights of the multiple nonlinear layers toward zero to approach identity mappings.”

In our study, we try to use Machine Learning to find gravitational candidates based on the spectroscopic-selection technique. The spectrum is one dimensional sequence and has local correlation. Therefore, we, of cause, use one dimensional CNNs to built the model, because CNNs shows good performance in distinguishing the input with local correlation. We also want to guarantee the accuracy of our selections by increasing the depth of the CNNs models, therefore, we adopt the Resnet model to prevent “degradation” problem and reduce the difficulty of training. In fact, before the final choice of Resnet, we have tried several “plain” networks (e.g., LeNet; AlexNet), but they are difficult to convergence in our problem.

3 USE RESNET TO FIND THE EMISSION LINES FROM HIGHER REDSHIFT

So far, several gravitational lens surveys based on spectroscopic-selection have been achieved (e.g., the SLACS, BELLS, S4TM and BELLS GALLERY). The SLACS, BELLS and S4TM surveys concentrated on searching multiple emissions, mainly the [OII] 3727 or [OIII] 5007 emissions coming from the galaxies with higher redshift than

the foreground galaxies, while BELLS GALLERY focused on just one higher redshift $\text{Ly}\alpha$ emissions. In our study, we use Resnet to find high redshift ($2 < z < 3$) $\text{Ly}\alpha$ emissions in the spectra of BOSS survey galaxies to search galaxy- $\text{Ly}\alpha$ emitter lens candidates. We don’t search the multiple [OII] 3727 or [OIII] 5007 emissions as SLACS have done because using just one emissions to build the train/test data is more simple. However, in the band ($3800\text{\AA} < \lambda < 5000\text{\AA}$, see it in Section 3.2) we choose, the spectra with lower redshift [OII] 3727 or other lower redshift emissions could also been found by our network. We will abundant these spectra trough several other subsequent selections (see it in Section 4).

3.1 the BELLS GALLERY survey

The lens candidates of BELLS GALLERY are selected from the DR12 of the BOSS of the SDSS-III by searching for $\text{Ly}\alpha$ emission lines from higher redshift $\text{Ly}\alpha$ emitters, and then following up high-resolution Hubble Space Telescope (HST) imaging observations to confirm the lens nature. In Shu et al. (2016a), the first and most important step is selecting out the spectra with emissions which are not from the target galaxies themselves. To do this, they confined their research to the observed wavelength range of $3600\text{\AA} < \lambda < 4800\text{\AA}$ (roughly $2 < z < 3$ for the $\text{Ly}\alpha$ emissions) and used an error-weighted matched-filter with a Gaussian kernel to search the $\text{Ly}\alpha$ emissions in BOSS targets. This mean step yielded 4982 hits. Then they performed several subsequent selections to reject the false hits and finally found 187 lens candidates with obvious $\text{Ly}\alpha$ emissions from higher redshift. They presented 21 highest quality BELLS GALLERY candidates in their paper, and among them 17 candidates have been confirmed to be gravitational lenses by HST imaging observations. The goal of the BELLS GALLERY survey is to exploit the small-scale dark substructure in the location of the lensed LAEs images and to constrain the slope and normalization of the substructure-mass function. As for why the galaxy-LAEs lens are suitable for constraining the substructure-mass function, Shu et al. (2016a) have discussed it carefully. Additionally, benefited from the magnifying effect of the gravitational lenses, the BELLS GALLERY samples also provide us good opportunities to study the LAEs themselves. LAEs is a kind of young, low-mass galaxies with extremely star-formation. They are an important component of the early universe, and are critical for studying the formation and evolution of galaxies at that time.

BELLS GALLERY is a successful lens candidates searching work. However, the first step of the selections is complex and consume too much time. First, they have to obtain an accurate estimate of the spectroscopic flux errors across the observed spectra; second, a standard spectroscopic template for ETGs is needed to fit each spectrum and obtain the galaxy-subtracted residual spectrum. For millions of targets, this procession would consume too much time. Therefore, In order to improve the selection speed of this step, we introduce the machine learning to automatically select out the spectra with emissions which are not from the targets themselves.

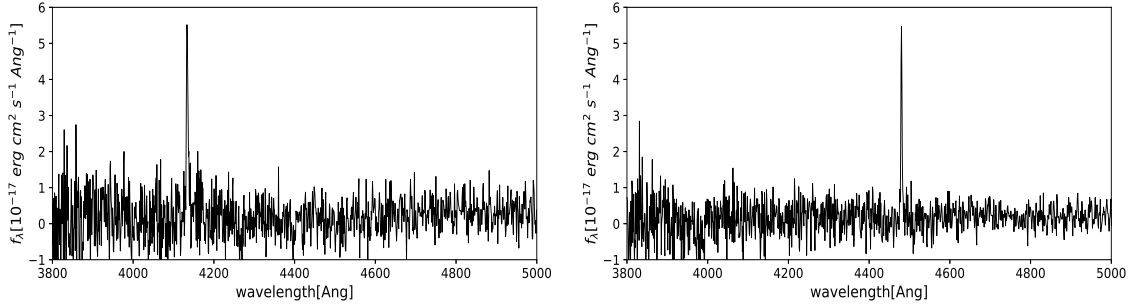


Figure 2. The left is the spectrum of SDSSJ 1110+2808 which comes from BELLS GALLERY. The right is an artificial one. Both are high SNR lines Ly- α

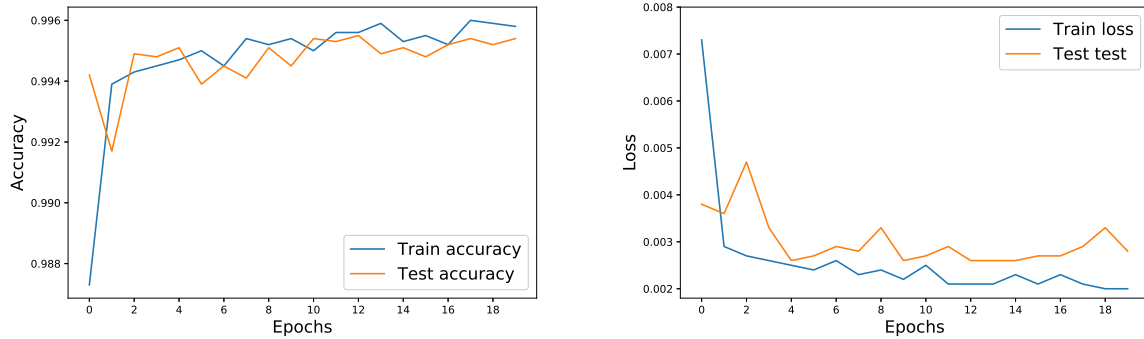


Figure 3. The left is the train/test accuracy. The right is the corresponding loss.

3.2 the predictive data and the train/test data

We aim to use a Resnet model to search galaxy-LAEs lens candidates from the DR12 of BOSS of SDSS-III based on spectroscopic-selection. We first take out all the ETGs spectra from the database to build our predictive data. The BOSS targets have been classified as several classes, such as "GALAXY", "SKY", "STAR". Therefore, we could choose the "GALAXY" class and filter out the targets with subclass keyword "STARFORMING", "BROADLINE" and "AGN". We then limit our selection to the redshift range of $z > 0.3$. These selections results in 1,241,799 recorders. For these recorders we then intercept the part ranged from 3800Å to 5000Å to build our predictive spectra. Notice that we don't use the same wavelength range as BELLS GALLERY ($3600\text{Å} < \lambda < 4800\text{Å}$), because we find that the wavelength ranged from 3600Å to 3800Å is very noisy, which could decrease the accuracy of our Resnet model.

Our predictive data include 177 known lens candidates from Shu et al. (2016a), the remaining 10 candidates in their work are eliminated because of the redshift limitation. Additionally, the Ly α emissions of 3 of the 177 candidates do not fall into the redshift range of $3800\text{Å} < \lambda < 5000\text{Å}$. Therefore, if we use this known lens candidates to test our Resnet model, just 174 candidates could be used.

Finding lens candidates in a great deal of galaxy spectra is a classification problem. Therefore, we use Resnet to build a classifier which could search the spectra with emissions coming from galaxies with higher redshift than the foreground lens galaxies. The quality of the train/test data

is very critical for the train/test accuracy of the classifier and directly affect the efficiency of the classification. For the train/test data, we require: 1.) the train/test data is not in the DR12 of BOSS of SDSS-III database, but looks like the spectra in it; 2.) the number of the train/test spectra have to be enough, usually more than ten thousands; 3.) the train/test data have been classified to two groups, one group has no Ly α emission (labeled [0]), and the other one has Ly α emission (labeled [1]); 4.) for the real spectra in DR12, the spectra with Ly α emissions are much less than the spectra without Ly α emissions, which makes serious data imbalance, therefore, a similar data imbalance should exists in the train/test data. So far, we just have no more than 200 galaxy spectra with Ly α emissions coming from higher redshift, which is far from enough. Therefore, we use the following procedure to build an artificial train/test data set.

(i) We grid the redshift to small bins ($\delta z = 0.0025$) and perform a Principal Component Analysis (PCA) to the whole spectra (roughly $3600\text{Å} < \lambda < 10300\text{Å}$) of ETGs (Chen et al. 2012; Shu et al. 2012) at each redshift bin. Then we use the first six eigenvectors of the PCA to create some artificial galaxy spectra at the corresponding redshift bin. Finally, we obtain totally 150,000 artificial galaxy spectra.

(ii) We add the "sky" and "noise" (coming from BOSS targets) to the created spectra and now the galaxy spectra looks like a real one. We then intercept the part ranged form 3800Å to 5000Å.

(iii) In the rest-frame wavelength, we use two Gaussian profiles to crate 10,000 artificial Ly α emissions. The mean

wavelength of the two Gaussian profiles is at 1216Å and the Full Width at Half Maximum (FWHM) is randomly obtained from a normal distribution with the mean value of $300\text{km} \cdot \text{s}^{-1}$ and standard deviation of $200\text{km} \cdot \text{s}^{-1}$. We then limit the FWHM greater than 0.5Å and limit the peak of the emission greater than $1.5 \times 10^{-17}\text{erg} \cdot \text{cm}^2 \cdot \text{Å}^{-1}$. Finally, we randomly shift them to the wavelength of $3800\text{Å} < \lambda < 5000\text{Å}$.

(iv) We randomly select 10,000 spectra from the totally 150,000 spectra and add the 10,000 artificial Ly α emissions to them, then label them [1]. The remaining spectra with no emissions are labeled [0]. The spectra with Ly α emissions are 1/15 of the total train/test spectra in order to overcome the classification imbalance of the real data in the BOSS data set.

Now, we have successfully built 150,000 train/test spectra. Notice that the PCA approach we performed in the first step will lose some information of the spectra. However, we point out that the lost information does not affect our training and results. On the one hand, the first 6 eigenvectors are enough to fit a real spectrum with an acceptable χ^2 . On the other hand, most of the lost information is the noise, after we add the "sky" and "noise" in the second step, the created spectrum looks exactly the same as a real one. Figure 2 shows two high SNR spectra of Ly- α emitters. the left one is the real spectrum of SDSS J1110+2808 (one of BELLS GALLERY samples) while the right is an artificial one with an synthetical Ly α emissions. They are look very similar. Another point we need to discuss is the Gaussian profile approximations for creating Ly α emissions. As we will show in Section 4, the Ly α emission is in fact skewed. However, in this study, we just want to use Resnet to recognise the emissions with any shapes. The shape judgement will be done by some other subsequent selections. Therefore, using skewed profiles to create Ly α is not necessary. During the experimentation, we find the Gaussian profile approximations can efficiently help us to find the emissions with any shapes.

3.3 Our Resnet model

Our Resnet model has 8 blocks, 28 Convolutional Layers, which is much deeper than a plain CNNs. We add a "Max-pooling" layer between any two blocks. A Dropout layer is employed before the fully connected layer in order to prevent over-fitting. As mentioned before, the samples labeled [1] are far less than the samples labeled [0], making a serious data imbalance. Here, we also add another measure—using the "Focal Loss" to overcome the effect of the data imbalance. The "Focal Loss" could be written as

$$L_{fl} = \begin{cases} -(1 - \hat{y})^y \log \hat{y} & \text{when } y = 1 \\ -\hat{y}^y \log(1 - \hat{y}) & \text{when } y = 0 \end{cases} \quad (1)$$

$y \in \{0, 1\}$ is the real label while \hat{y} is the prediction value. The "Focal Loss" is designed to improve the classifying task with an extreme data imbalance, which is described detailedly in Lin et al. (2017).

We finally apply our program to the train/test data (the ratio of the train data and test data is 9 : 1). In the training process, we mask the location of [NeV] 3347, [NeV] 3427, [OII] 3727 and [NeIII] 3869, which may comes

from the ETGs themselves. The output of our program for each spectrum is the probability to be a lens candidate. We treat the samples with probability greater than 0.5 as lens candidates. Figure 3 shows the accuracy and loss of the train/test data. We obtain a perfect test accuracy of 0.9954, and the corresponding loss is 0.0028. After successfully training the Resnet model, we apply the model to our predictive data (the emissions of the ETGs themselves also have been masked). We successfully find all the 21 BELLS GALLERY lens candidates with the possibilities extremely close to 1. As for all the 174 known lens candidates in our predictive spectra, we could find 161 of them. The discovery rate is 92.5%.

4 OUR STRONG GRAVITATIONAL LENSING CANDIDATES

We totally find 1232 hits using our Resnet model, including 161 candidates which have been found in Shu et al. (2016a). Apart from the hits existing in the 4982 hits of BELLS GALLERY, we also find another 536 hits. Then we perform several subsequent selections similar Shu et al. (2016a) remove the false hits. In order to ensure the higher quality, we first apply a visual inspection to the 536 hits and reject the samples with too much noise and very lower emission lines (the peak value of the emission flux is about less than $1 \times 10^{-17}\text{erg} \cdot \text{cm}^2 \cdot \text{Å}^{-1}$). This cut removes most of the hits and left 124 hits. For these 124 hits, we remove the hits with significant numerical over-densities in both observed wavelength (associated with airglow features, Shu et al. (2016a)) and BOSS target-galaxy rest wavelength (associated with template-subtraction residuals). This step remove 77 spurious hits.

We know that one typical feature of high redshift Ly α emissions is the "blue edge, red tail" profiles (see it in BELLS GALLERY samples). Therefore, we use the skew normal profiles to fit the emissions of the remain 47 hits and finally left 22 samples with skewness parameter bigger than 0. This fitting is achieved by non-linear least squares. During the fitting process, all of the 4 necessary parameters (the Skewness, mean value, Standard Deviation and kurtosis) describing a skew normal profiles are varied. Additionally, the noise of the spectra which provided by SDSS is stationary.

We then remove 16 samples with low-redshift [OII] emissions. In this step, we suppose the emissions is [OII] emissions and calculate the relative positions of OIII, H α and H β emissions. If any of these positions has an emission, we reject the sample. Finally, we obtain 6 LAEs lens candidates and all the properties of these 6 candidates are shown in Table 1. We also show the emission profiles and their best fitting skew normal profiles in Figure 4. Among the 6 lens candidates, the Ly α emissions of 1 samples (SDSS J153520.91+235221.7) fall into the redshift range of $4800\text{Å} < \lambda < 5000\text{Å}$, which is higher than BELLS SAMPLES.

5 DISCUSSION AND IMPROVEMENT

Comparing with Shu et al. (2016a), we find about an equal number of lens candidates (161+6) in the same database (DR12 of BOSS) using Machine Learning. However, the

Table 1. Selected properties of the 6 galaxy-LAE lens candidate systems.

Target	Plate-MJD-Fiber	z_L	z_s	R.A.	Decl.	m_i	Ly α Flux
SDSS J111749.50+014036.9	4731-55656-197	0.5840	2.1570	11:17:49.50	+01:40:36.95	19.35	30.4
SDSS J121650.13+500700.2	6671-56388-589	0.6613	2.7894	12:16:50.13	+50:07:00.26	19.83	36.7
SDSS J122502.89-000907.8	3847-55588-309	0.4868	2.4395	12:25:02.89	-00:09:07.85	19.61	12.3
SDSS J142310.55+231928.1	6013-56074-66	0.4717	2.4099	14:23:10.55	+23:19:28.17	19.66	50.8
SDSS J143428.11+470111.5	6736-56366-505	0.5070	2.3913	14:34:28.11	+47:01:11.53	19.25	24.2
SDSS J153520.91+235221.7	3948-55331-685	0.4945	2.9754	15:35:20.91	+23:52:21.79	19.3	7.2

NOTE. — Column 1 is the SDSS system name in terms of truncated J2000 R.A and decl. in the format HHMMSS.ss± DDMMS.s. Column 2 provides the plate-MJD-fiber of the spectra. Columns 3 and 4 are the redshifts of the foreground lenses and the background galaxies inferred from the BOSS spectra. Column 5 and 6 is the coordinate in terms of truncated J2000 R.A and decl. Column 7 is the BOSS-measured i -band apparent cmodel magnitude within the 1'' fiber. And column 8 is the total apparent flux of the Ly α emission in units of $10^{-17} \text{ erg} \cdot \text{cm}^{-2} \cdot \text{s}^{-1}$.

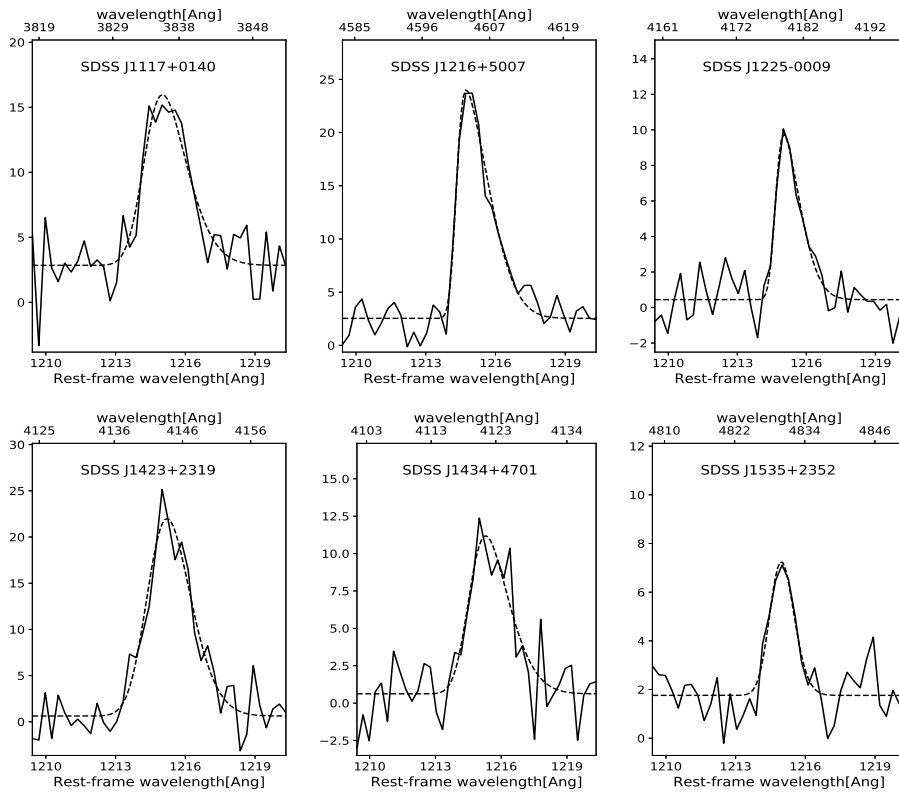


Figure 4. Zoomed in views of the Ly α emission lines for the candidates ordered by decreasing apparent Ly α flux, de-redshifted to the rest frame of the LAEs. Dashed lines are the best-fit continuum flux for the Ly α emissions using skew normal distribution. Note the "blue edge, red tail" line profiles characteristic of LAEs.

recognition speed of our strategy is much higher than that of theirs. After successfully training the model, we can finish the recognition process within just an hour and a half using the CPU (Central Processing Unit) of a common laptop computer. By contrast, the method used in [Shu et al. \(2016a\)](#) needs about 10 hours to finish a similar recognition. Computing on GPU (Graphic Processing Unit) could effectively increase the recognition speed, usually 5 to 10 times as compared with computing on CPU. Although we have not tried the GPU computation, we can expect that the recognition could be finished within about 20 minutes, much faster than the method in [Shu et al. \(2016a\)](#). This advantages would become more and more important with the arrival of big data age of astronomy. It is worth noting that the

recognition process we discussed above doesn't include the training process. Although we have to spend several hours to train the network in the beginning, our strategy is still a high-efficiency one, because after the network has been successfully trained, it can be used to any other predictive data without retraining.

This work is just the first attempt to find lens candidates with Resnet based on spectroscopic-selection. Our strategy still has very large development space. The first problem to be overcome is the noise. During the repeating experiments, we find the spectra with too much noise could decrease our accuracy, that is why we reject the wavelength range of $3600\text{\AA} < \lambda < 3800\text{\AA}$. The second problem is the subsequent selection. Our Resnet can successfully find the

the spectra with emissions coming from a different redshift, but it can not judge they are $\text{Ly}\alpha$ emissions coming from higher redshift or [OII] emissions coming from lower redshift. Therefore, after the Resnet selection, a subsequent selection which have been used in previous work is needed. If we want to directly find the emissions with skewness bigger than 0, building the emissions with skewed profile and classifying the train data to 3 class is an alternative approach. The first class is the spectra with no emissions, the second is the spectra with skewed emissions which have negative skewness and the third is the spectra with skewed emission which have positive skewness. However, this approach still need subsequent selection and seems unnecessary in this work. Another alternative method is to use a regression Resnet model to give the redshift of the source galaxies. This method requires the whole spectrum. We hope the regression model could learn the redshift of the source through the relative position of multiple emissions. However, for a regression model, to overcome the data imbalance is more difficult than a classification model.

6 CONCLUSIONS

In this work, We have successfully applied the Resnet model to the search for galaxy- $\text{Ly}\alpha$ emitter lens candidates in DR12 of the BOSS of SDSS-III based on spectroscopic-selection. We use 140,000 spectra without $\text{Ly}\alpha$ emissions and 10,000 ones with $\text{Ly}\alpha$ emissions to train a 28 layers Resnet model and get a perfect test accuracy of 0.9954 with the corresponding loss of 0.0028. After we apply our Resnet model to the 1,241,799 predictive spectra coming from the DR12 of the BOSS of SDSS-III, we totally find 1232 hits, including 161 known lens candidates. Considering that, for all the 187 known candidates in Shu et al. (2016a), there are only 177 spectra in our predictive data and the $\text{Ly}\alpha$ emissions of 3 fall outside the wavelength range of $4800\text{\AA} < \lambda < 5000\text{\AA}$. We actually could find 92.5% of them. Finally, we perform several subsequent selections to another 536 hits which are not found in Shu et al. (2016a) and find 6 new galaxy- $\text{Ly}\alpha$ emitter lens candidates.

The most obvious advantage of our strategy based on Machine Learning is the recognition speed. Comparing with previous work (Shu et al. 2016a), we find a similar number of lens candidates in the same database, but with much less time. For Resnet, the GPU computation would consume much less time than the CPU computation. Although we have not compute our model on GPU because of the lack of a suitable device, but we expect that a suitable GPU device could finish the selection within 20 minutes. This work is just the first attempt to find lens candidates using Machine Learning. We will continue to improve the strategy and build a perfect method to search galaxy-scale lens candidates using Machine Learning.

7 ACKNOWLEDGEMENT

We acknowledge the financial support from the National Natural Science Foundation of China 11573060 and 11661161010. Y.S. has been supported by the National Natural Science Foundation of China (No. 11603032 and

11333008), the 973 program (No. 2015CB857003), and the Royal Society     K.C. Wong International Fellowship (NF170995).

REFERENCES

- A. Krizhevsky, I. Sutskever, and G. Hinton. Advances in neural information processing systems, page 1097–1105. (2012)
- Auger, M. W., Treu, T., Bolton, A. S., et al. 2009, ApJ, 705, 1099
- Auger, M. W., Treu, T., Bolton, A. S., et al. 2010, ApJ, 724, 511
- Bolton, A. S., Burles, S., Schlegel, D. J., Eisenstein, D. J., & Brinkmann, J. 2004, AJ, 127, 1860
- Bolton, A. S., Burles, S., Koopmans, L. V. E., Treu, T., & Moustakas, L. A. 2006, ApJ, 638, 703
- Bolton, A. S., Burles, S., Koopmans, L. V. E., et al. 2008, ApJ, 682, 964-984
- Bolton, A. S., Brownstein, J. R., Kochanek, C. S., et al. 2012, ApJ, 757, 82
- Brownstein, J. R., Bolton, A. S., Schlegel, D. J., et al. 2012, ApJ, 744, 41
- Dawson, K. S., Schlegel, D. J., Ahn, C. P., et al. 2013, AJ, 145, 10
- Dieleman, S., Willett, K. W., & Dambre, J. 2015, MNRAS, 450, 1441
- Eisenstein, D. J., Weinberg, D. H., Agol, E., et al. 2011, AJ, 142, 72
- Gavazzi, R., Marshall, P. J., Treu, T., & Sonnenfeld, A. 2014, ApJ, 785, 144
- Gehring, J., Auli, M., Grangier, D., Yarats, D., & Dauphin, Y. N. 2017, arXiv:1705.03122
- H  la, P. 2014, arXiv:1412.8341
- He, K., Zhang, X., Ren, S., & Sun, J. 2015, arXiv:1512.03385
- Horesh, A., Ofek, E. O., Maoz, D., et al. 2005, ApJ, 633, 768
- Hoyle, B. 2016, Astronomy and Computing, 16, 34
- Impellizzeri, C. M. V., McKean, J. P., Castangia, P., et al. 2008, Nature, 456, 927
- Joseph, R., Courbin, F., Metcalf, R. B., et al. 2014, A&A, 566, A63
- Lenzen, F., Schindler, S., & Scherzer, O. 2004, A&A, 416, 391
- Lecun, Y. & Bottou, L. & Bengio, Y. & Haffner, P. (1998). Proceedings of the IEEE. 86. 2278 - 2324. 10.1109/5.726791.
- Lin, T.-Y., Goyal, P., Girshick, R., He, K., & Doll  r, P. 2017, arXiv:1708.02002
- Kim, E. J., & Brunner, R. J. 2017, MNRAS, 464, 4463
- Kubo, J. M., & Dell’Antonio, I. P. 2008, MNRAS, 385, 918
- Koopmans, L. V. E., & Treu, T. 2003, ApJ, 583, 606
- Koopmans, L. V. E., Treu, T., Bolton, A. S., Burles, S., & Moustakas, L. A. 2006, ApJ, 649, 599
- Koopmans, L. V. E., Bolton, A., Treu, T., et al. 2009, ApJ, 703, L51
- Koopmans, L. V. E., & Treu, T. 2003, ApJ, 583, 606
- Meyer R. A., Delubac T., Kneib J.-P., Courbin F., 2017, arXiv, arXiv:1711.01184
- More, A., Cabanac, R., More, S., et al. 2012, ApJ, 749, 38
- Navarro, J. F., Frenk, C. S., & White, S. D. M. 1996, ApJ, 462, 563
- Petrillo, C. E., Tortora, C., Chatterjee, S., et al. 2017, MNRAS, 472, 1129
- Ruff, A. J., Gavazzi, R., Marshall, P. J., et al. 2011, ApJ, 727, 96
- Shu, Y., Bolton, A. S., Schlegel, D. J., et al. 2012, AJ, 143, 90
- Shu, Y., Bolton, A. S., Brownstein, J. R., et al. 2015, ApJ, 803, 71
- Shu, Y., Bolton, A. S., Kochanek, C. S., et al. 2016, ApJ, 824, 86
- Shu, Y., Bolton, A. S., Mao, S., et al. 2016, ApJ, 833, 264
- Suyu, S. H., Auger, M. W., Hilbert, S., et al. 2013, ApJ, 766, 70
- Seidel, G., & Bartelmann, M. 2007, A&A, 472, 341
- Sonnenfeld, A., Treu, T., Gavazzi, R., et al. 2013, ApJ, 777, 98

- Treu, T., & Koopmans, L. V. E. 2004, ApJ, 611, 739
- Treu, T., Dutton, A. A., Auger, M. W., et al. 2011, MNRAS, 417, 1601
- Treu, T., Schmidt, K. B., Brammer, G. B., et al. 2015, ApJ, 812, 114
- Suyu, S. H., Auger, M. W., Hilbert, S., et al. 2013, ApJ, 766, 70
- Swinbank, A. M., Webb, T. M., Richard, J., et al. 2009, MNRAS, 400, 1121
- Warren, S. J., Hewett, P. C., Lewis, G. F., et al. 1996, MNRAS, 278, 139
- Chen, Y.-M., Kauffmann, G., Tremonti, C. A., et al. 2012, MNRAS, 421, 314